

## Article

# Advancing Manganese Content Prediction in Submerged Arc Welded Metal: Development of a Multi-Zone Model via the Calphad Technique

Jin Zhang <sup>1,2</sup>, Ping Liu <sup>1</sup> and Dan Zhang <sup>3,\*</sup><sup>1</sup> School of Mechanical and Electrical Engineering, Suqian University, Suqian 223800, China<sup>2</sup> School of Metallurgy, Northeastern University, Shenyang 110819, China<sup>3</sup> Department of Science and Technology, Suqian University, Suqian 223800, China

\* Correspondence: 90026@squ.edu.cn

**Abstract:** Manganese is a vital element in determining the mechanical properties of submerged arc welded metal. To ensure a reliable weld, the equilibrium model has been used for decades to predict and control the manganese content, particularly when MnO-bearing fluxes are applied. However, the equilibrium model only considers chemical interactions within the weld pool zone, leading to significant inaccuracies. To address this limitation, we propose a multi-zone model that accounts for all of the essential reaction zones in the submerged arc process via the Calphad technique. The model's accuracy is verified by predicting the manganese content, the flux oxygen potential, and the neutral point location for the typical MnO-bearing fluxes covering acidic, neutral, and basic fluxes. The results indicate that the multi-zone model offers superior accuracy compared to the equilibrium model, which neglects significant oxygen improvement and alloy evaporation in the droplet zone. Further analysis of thermodynamic data reveals that the multi-zone model provides a more representative depiction of the variation trends in oxygen and manganese contents during the submerged arc welding process compared to the equilibrium model. Furthermore, this model can be utilized in the optimization of the submerged arc welding process, leading to improved quality and efficiency in heavy engineering industries. This study may provide an improved method for predicting the manganese content in welded C-Mn steel and deepen the understanding of manganese transfer mechanisms during the submerged arc welding process.

**Keywords:** submerged arc welding; welding process; chemical reactions; equilibrium principles; gas–slag–metal equilibrium; compositional control



**Citation:** Zhang, J.; Liu, P.; Zhang, D. Advancing Manganese Content Prediction in Submerged Arc Welded Metal: Development of a Multi-Zone Model via the Calphad Technique. *Processes* **2023**, *11*, 1265. <https://doi.org/10.3390/pr11041265>

*Processes* **2023**, *11*, 1265. <https://doi.org/10.3390/pr11041265>

Academic Editor: Chin-Hyung Lee

Received: 29 March 2023

Revised: 13 April 2023

Accepted: 14 April 2023

Published: 19 April 2023



**Copyright:** © 2023 by the authors. Licensee MDPI, Basel, Switzerland. This article is an open access article distributed under the terms and conditions of the Creative Commons Attribution (CC BY) license (<https://creativecommons.org/licenses/by/4.0/>).

## 1. Introduction

The process of submerged arc welding (SAW) is ideal for welding thick workpieces [1–3]. Due to its excellent reliability and high deposition rate, SAW is extensively employed in heavy engineering sectors [1–3]. The arc plasma and weld pool in SAW are concealed by a layer of flux, making them invisible during the welding process [4–8]. Submerged arc welding is a complex metallurgical process that involves temperatures exceeding 1900 °C, which enables chemical interactions among the different phases that are involved, such as the arc plasma, flux/slag, and molten metal. These interactions can lead to compositional changes within the metal, which in turn affect the mechanical properties and the overall quality. Therefore, the proper control of the compositions and the selection of appropriate fluxes are crucial for achieving the desired weld quality and ensuring the long-term performance of the welded structure [9–14].

MnO-bearing fluxes are widely applied in SAW engineering to fine tune the weld metal (WM) manganese content [3,4,15]. Manganese is a fundamental element pertinent to WM microstructures and mechanical properties [16,17]. It has been revealed that the gradual increase in manganese content, from 0.6 to 1.8 wt pct, can promote the formation

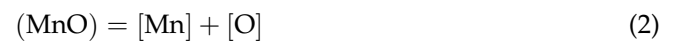
of acicular ferrite (a microstructure that is inherently intertwined, providing an optimum combination of strength and toughness) and inhibit the formation of brittle microstructures, such as polygonal and side plate ferrites [18–20].

Equilibrium is typically difficult to achieve during the SAW process due to factors such as significant temperature gradients, the presence of various phases, and the high energy that is transferred from the plasma [4,5]. Nevertheless, despite these deviations, it is still possible to apply equilibrium principles in order to establish constraints on the chemical mechanisms and interactions in the SAW process by assuming that local equilibrium can be achieved due to the high temperatures and surface-to-volume ratios that are involved [15,21]. Hence, although complete equilibrium may not be reached in the SAW process, the use of local equilibrium principles can still offer valuable information regarding the chemical mechanisms and reactions, thereby assisting in the enhancement of the welding process.

Chai et al. [16,17,22] have developed the slag–metal equilibrium model as the initial thermodynamic model using the following approaches:

1. The WM oxygen content ([pct O]) is predicted from the flux basicity index (BI, an empirical indicator that is used to estimate the WM oxygen content), as illustrated by Equation (1) [23].
2. By using Equation (3), the manganese content is predicted from the oxygen content in WM, the MnO activity ( $\alpha_{\text{MnO}}$ ) in flux, and the equilibrium constant of Reaction (2), which governs the transfer behaviors of manganese and oxygen at the slag–metal interface.

$$BI = \frac{\text{CaO} + \text{CaF}_2 + \text{MgO} + \text{K}_2\text{O} + \text{Na}_2\text{O} + \text{Li}_2\text{O} + 1/2(\text{MnO} + \text{FeO})}{\text{SiO}_2 + 1/2(\text{Al}_2\text{O}_3 + \text{TiO}_2 + \text{ZrO}_2)} \quad (1)$$



$$[\text{pct Mn}] = \frac{\alpha_{\text{MnO}}}{0.86 \cdot [\text{pct O}]} \quad (3)$$

In subsequent research, scholars have highlighted the inherent shortcomings of the slag–metal equilibrium model, which stem from the absence of fundamental links between the flux composition and the oxygen potential [4,5]. More recently, the gas–slag–metal equilibrium model has been developed as an improvement over the slag–metal equilibrium model [10,12,24]. This updated model has been shown to enhance the accuracy of manganese content predictions [12]. Nonetheless, the gas–slag–metal equilibrium model is constrained to the equilibrium conditions prevailing solely within the weld pool zone, and predictive errors still persist for several reasons [10], as follows:

1. Manganese is a special element for SAW, due to its tendency to evaporate in the arc cavity (droplet zone).
2. The significant improvement of oxygen concentration in the droplet tends to induce the loss of manganese via oxidation reactions, due to manganese being a strong deoxidizer (droplet zone).
3. During cooling and solidification, manganese is redistributed within the welded metal.

Typically, the SAW process can be categorized into the following three zones: the droplet zone, the weld pool zone, and the solidification zone. Considering the possible change in the metal composition at various stages of the SAW process, comprehensive considerations of the SAW process are necessary to ensure model precision [25–27]. The objective of the current investigation is to establish a multi-zone model that considers the essential chemical reaction zones within the welding process, including the droplet, weld pool, and solidification zones. The developed multi-zone model takes into account the complex chemical reactions and the transfer behavior of manganese and oxygen, which are critical factors in determining the microstructure and the mechanical properties of the

welded metal. The prediction data are to be verified with the typical MnO-bearing fluxes, viz.  $\text{CaF}_2\text{-SiO}_2\text{-Na}_2\text{O-MnO}$  fluxes, with a wide range of MnO content at full coverage with acidic, neutral, and basic fluxes. Then, the prediction capability of the multi-zone model is evaluated, and the transfer behavior of manganese and oxygen is interpreted. In order to evaluate the validity of the prediction results, the changing trend of elemental transfer during the SAW process is discussed.

## 2. Material and Methods

### 2.1. Flux Design

The metal must be shielded from the atmosphere with a flux during SAW. Therefore, the melting temperature of the flux should be controlled under  $1500\text{ }^\circ\text{C}$  to guarantee that the molten metal solidifies prior to the solidification of the molten slag [5,28]. In order to ensure the appropriate melting temperature of the flux, a graph of the isotherm projection for  $\text{CaF}_2\text{-SiO}_2\text{-MnO}$  melts was plotted, as shown in Figure 1 [29]. To ensure a broad scope of MnO addition in the design, the content of  $\text{SiO}_2$  was maintained at 40 wt pct [15]. The MnO content varied from 0 to 60 wt pct in increments of 10 wt pct, with  $\text{CaF}_2$  constituting the remaining portion, in order to determine the appropriate formula for each flux. The acceptable melting temperature can be observed in Figure 1, where each flux formula is represented by a red dot.

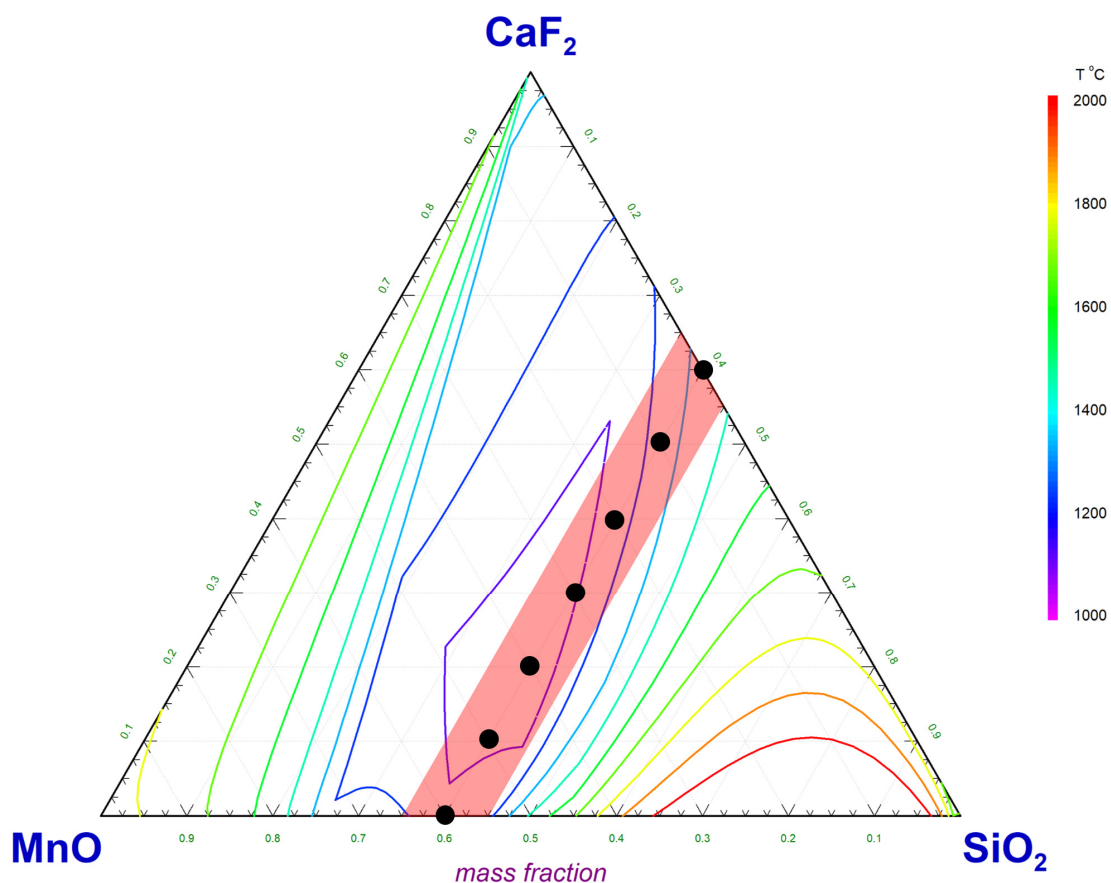


**Figure 1.** Isotherm projection graph for  $\text{CaF}_2\text{-SiO}_2\text{-MnO}$  melts.

Based on the flux formulas given in Figure 1, a trace of  $\text{Na}_2\text{O}$  was incorporated, since it helps to improve the arc stability. The concentration of  $\text{Na}_2\text{O}$  was determined based on typical commercial fluxes [3].

The base metal (BM) chosen for this study was Q345A, a typical low alloy C-Mn steel. Bead-on-plate double-electrodes single-pass SAW was conducted using a heat input of  $60\text{ kJ/cm}$  (with DC-850 A/32 V for electrode forward and AC-625 A/36 V for electrode

backward, at a speed of 500 mm/min) and 20 kJ/cm (with DC-436 A/30 V, at a speed of 393 mm/min). The choice of the bead-on-plate welding configuration was made to facilitate the quantification of the element transfer behavior in welding. The selection of high heat input welding was made to bring the SAW system closer to thermodynamic equilibrium status.

To evaluate the validity of the results, the selected welding flux is a typical and commonly used silicon–manganese type [4]. The MnO composition range is guaranteed to be very wide, covering acidic, neutral, and basic fluxes. By combining thermodynamic data, the flux is ensured to meet the basic requirements of flux design. To ensure arc stability, Na<sub>2</sub>O was added to the flux [3]. More information on the welding procedure, as well as the specific compositions of the fluxes and metals used, can be found in our previous study [3]. Tables 1 and 2 provide a summary of the compositions of the fluxes, base metal (BM), and electrode.

**Table 1.** Measured compositions of the fluxes (wt pct) [3].

Flux	CaF <sub>2</sub>	Na <sub>2</sub> O	SiO <sub>2</sub>	MnO	BI	Type
F-0	60.08	1.23	38.69	0	1.58	Basic
F-1	48.40	1.24	40.15	10.21	1.36	Basic
F-2	36.79	1.21	41.22	20.78	1.17	Neutral
F-3	29.50	1.19	39.45	29.86	1.16	Neutral
F-4	18.89	1.31	38.68	41.12	1.05	Neutral
F-5	10.15	1.18	38.13	50.54	0.96	Acidic
F-6	0	1.29	40.53	58.18	0.75	Acidic

**Table 2.** Measured chemical compositions of the BM and electrode (wt pct) [3].

	C	Si	Mn	Ti	Al	O
<b>BM</b>	0.113	0.142	1.54	0.01	0.12	0.003
<b>Electrode</b>	0.127	0.138	1.65	0.01	0.14	0.003

## 2.2. Modeling Approach

Calphad is an abbreviation for computer coupling of phase diagrams and thermochemistry. It employs thermodynamic models to predict the properties of material systems with a higher order, based on basic thermodynamic data of binary and/or ternary material systems [29]. Since the temperatures are higher than 1900 °C during SAW, it is impossible to directly measure the thermodynamic data [4,10]. In spite of this constraint, the thermodynamic models employed in the Calphad approach have proven to be dependable in obtaining thermodynamic data at temperatures that surpass 1900 °C [29,30]. Given that SAW is a metallurgical system with multiple phases and ultra-high temperatures, the Calphad technique is utilized in this study to simulate the chemical interactions within the welding system [24,30].

## 3. Assumptions

As shown in Figure 2, the SAW process is usually categorized into three zones (droplet zone, weld pool zone, and solidification zone) based on the nature of the chemical interactions that occur [9,26]. The details subject to each zone in Figure 2 are elucidated below.

### 3.1. Droplet Zone—Figure 2b

Within this zone, the droplet separates from the electrode tip and travels through the arc cavity [26]. The initial experiments concluded that there was a negligible transfer of alloy elements within this zone [25]. It is hypothesized that the formation of an active O layer on the droplet prevents the alloying elements from reaching the metal–plasma interface, as illustrated by the green line around the droplet in Figure 2b [26]. Therefore, only the improvement of the O concentration is expected in this zone [27].

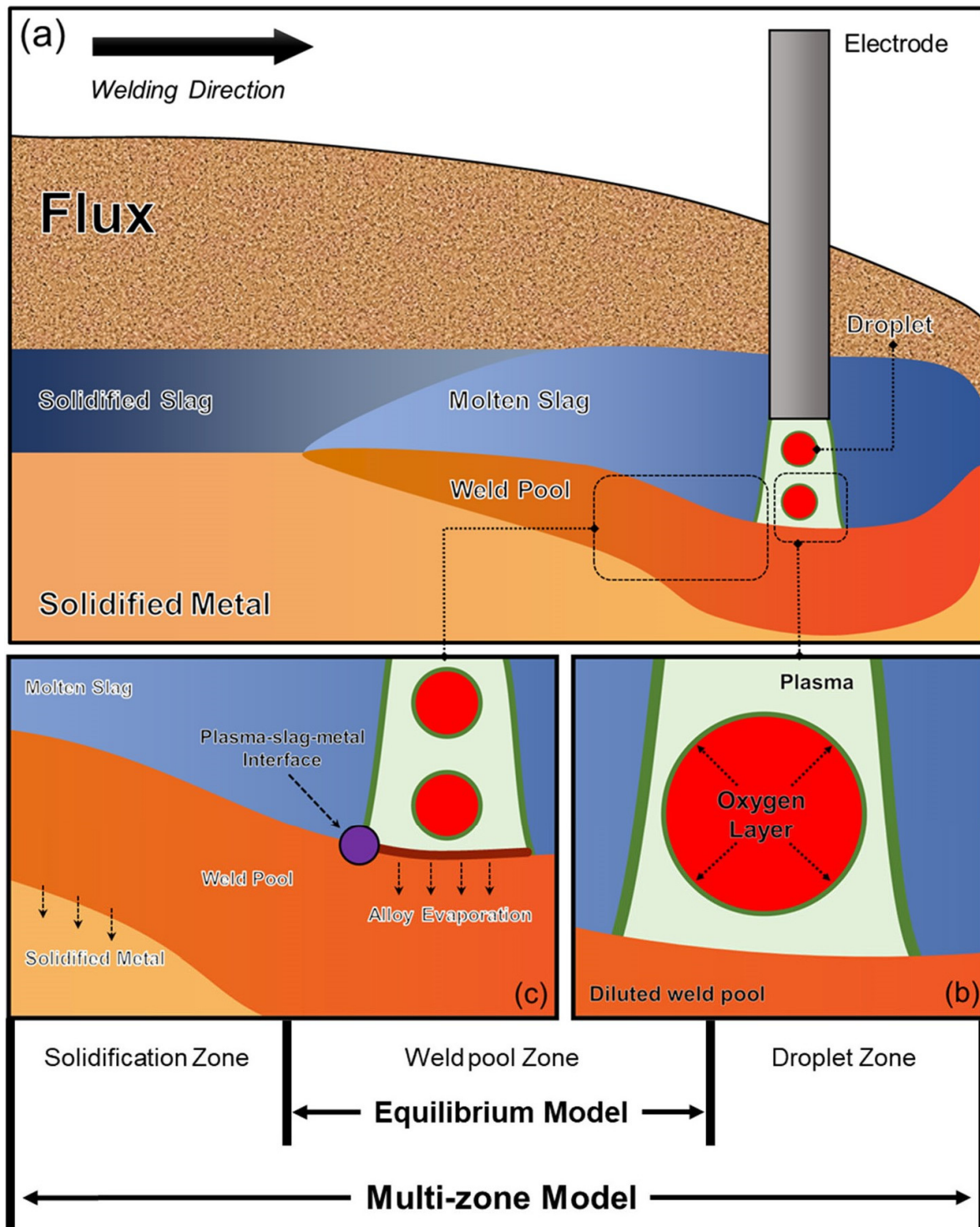


**Figure 2.** Reaction zones that control the manganese content in WM: (a) overall schematic diagram of submerged arc welding, (b) chemical reactions in droplet zone, and (c) chemical reactions in weld pool and solidification zones.

### 3.2. Weld Pool Zone—Figure 2c

Within this zone, the droplet is diluted by the BM [1]. The high temperature and the large convective forces induce the mixing of the molten metal and chemical interactions between the different phases, as shown in Figure 2c. After the droplet is diluted, chemical interactions take place at the plasma–slag–metal interface. Subsequently, the slag and the

liquid melt gradually solidify. It is noted that the evaluation of manganese is enabled in this zone.

### 3.2.1. Dilution Model

The nominal composition refers to the composition considering only the physical dilution of the BM and the electrode [4,15]. The nominal composition (nominal comp.) is calculated by Equation (4), where  $d_{BM}$  represents the dilution value of the BM (Chai et al., concluded that  $d_{BM}$  can be assumed to be 0.5 for thermodynamic calculations), BM comp. indicates the composition of BM, and electrode comp. indicates the composition of the electrode [10]. For equilibrium models, the nominal composition is typically set as the input chemistries of the metal [10,16].

However, as is demonstrated in Section 3.1, there is a significant improvement in the droplet O concentration. Thus, the calculation of the nominal composition is updated from Equation (4) to Equation (5), considering the improvement of the O concentration in the droplet zone.

$$\text{nominal comp.} = d_{BM} \times \text{BM comp.} + (1 - d_{BM}) \times \text{electrode comp.} \quad (4)$$

$$\text{nominal comp.} = d_{BM} \times \text{BM comp.} + (1 - d_{BM}) \times \text{droplet comp.} \quad (5)$$

### 3.2.2. Alloy Evaporation Model

During the arc welding process, it is inevitable that manganese and silicon will evaporate before the hot metal is submerged by the slag [1]. Various investigations have shown that relying solely on thermodynamics is insufficient to accurately predict the degree of alloy evaporation that takes place within this zone [28,31]. Recently, Zhu et al. [32] developed models to predict the loss of manganese and silicon due to evaporation at the plasma–metal interface induced by the plasma, based on the Langmuir Equation for C–Mn steel. Their results indicate that the predicted levels of manganese and silicon align well with the measured values. In this study, Zhu’s models are employed to estimate the loss of manganese and silicon at the plasma–metal interface, as shown by Equations (6) and (7), where  $\eta$  indicates the mass percentage and  $m$  indicates the nominal compositions of manganese and silicon [32].

$$\eta_{Mn} = 49.04 - 0.23m_{Mn} - 0.49m_{Si} \quad (6)$$

$$\eta_{Si} = 38.55 - 0.33m_{Mn} - 0.58m_{Si} \quad (7)$$

### 3.2.3. Equilibrium Model

The transfer of manganese at the gas–slag–metal interface within the weld pool zone is estimated using the gas–slag–metal equilibrium model, as depicted in Figure 2c. This model has been elaborated upon in previous works [10].

### 3.3. Solidification Zone

In the solidification zone, the hot metal begins to cool and solidify. Due to the increasing stability of oxides at lower temperatures, there is a slight decrease in the manganese content near the slag–metal interface, induced by the shifting of Reaction (2) to the left side [25,33]. However, since the manganese content primarily indicates the bulk compositions in the metal (not at the interface), this loss is neglected during the modeling process, as previously concluded [3,25].

## 4. Results and Discussion

In this study, Factsage, a thermodynamic software based on the Calphad technique, is employed for modeling purposes. This software includes multiple modules that are designed to manipulate thermodynamic data from various databases [29]. Specifically, the Fstel, FactPS, and FToxide modules are used to model the steel phase, gas phases, and

flux/slag phase, respectively. The Equilib module is employed to conduct thermodynamic equilibrium calculations, which involve determining the concentrations of chemical species when elements or compounds attain a state of chemical equilibrium [29].

The flowchart of the modeling process, along with the thermodynamic databases utilized, is illustrated in Figure 3. The model calculation process diagram in Figure 3 consists of a series of interconnected stages that represent the flow of data and the sequence of operations that are performed during the calculation process. The flowchart begins with an initial input stage, followed by a series of processing steps, and ends with a final output stage. The orange labeling represents the welding zone and the main scientific hypothesis corresponding to each stage. The blue labeling represents each sub-model used. The yellow labeling represents the thermodynamic databases employed, with details given in previous study [29]. The label “FactSage Equilib Module” represents the tools to perform the thermodynamic equilibrium calculation.

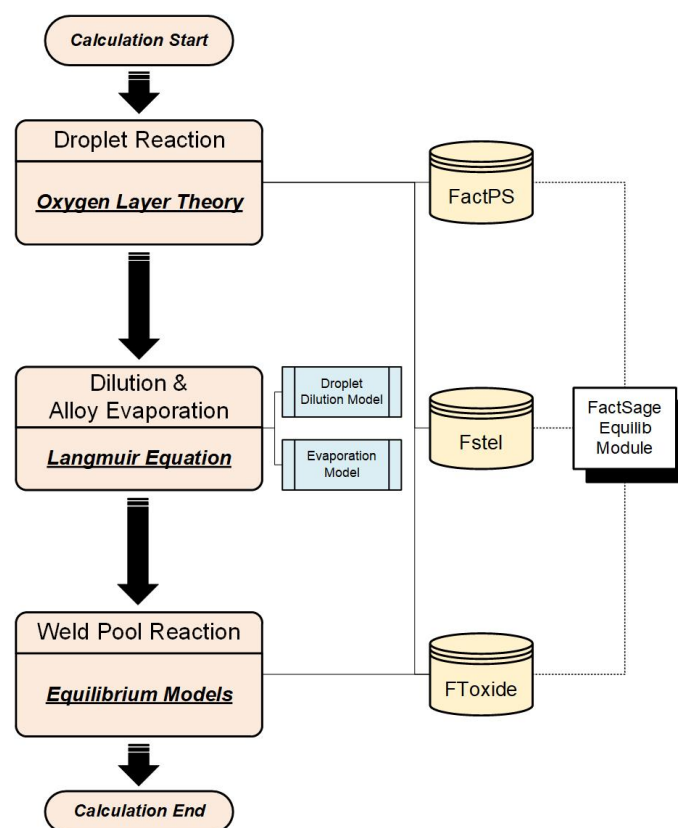


**Figure 3.** The process of modeling and the selection of thermodynamic databases.

#### 4.1. Droplet Reaction

The Equilib module is used to perform the modeling as follows [27]:

1. The FToxid, Fstel, and FactPS databases were chosen to be utilized. The solution phases of ASlag-liq all oxides, S (FToxid-SLAGH), and LIQUID (FStel-Liqu) were chosen to simulate the molten slag and steel phases.
2. The equilibrium temperature for the SAW process was set at 2500 °C, which corresponds to the temperature of the arc plasma. The input metal chemistries were based on the BM compositions.
3. To replicate the oxygen concentration in the droplet, an equilibrium calculation was performed, with iron and oxygen as the input metal components. The  $PO_2$  value provided in Table 3 was used in this process. Table 3 summarizes the simulated  $PO_2$  and oxygen concentration in the droplet that were obtained as the output.

**Table 3.** Output of simulated  $P_{O_2}$  (atm) and O concentration (wt pct) in the droplet.

Flux	$P_{O_2}$	O Concentration in Droplet
F-0	$1.25 \times 10^{-5}$	$4.66 \times 10^{-1}$
F-1	$1.36 \times 10^{-5}$	$4.86 \times 10^{-1}$
F-2	$1.38 \times 10^{-5}$	$4.90 \times 10^{-1}$
F-3	$1.32 \times 10^{-5}$	$4.79 \times 10^{-1}$
F-4	$1.21 \times 10^{-5}$	$4.59 \times 10^{-1}$
F-5	$1.08 \times 10^{-5}$	$4.33 \times 10^{-1}$
F-6	$9.67 \times 10^{-6}$	$4.10 \times 10^{-1}$

#### 4.2. Dilution and Alloy Evaporation

- Equation (5) is utilized to calculate the nominal compositions.
- Equations (6) and (7) are utilized to predict the loss of manganese and silicon due to evaporation. The calculated nominal compositions are given in Table 4.

**Table 4.** Nominal composition considering droplet dilution and evaporation (wt pct).

Flux	C	Si	Mn	Ti	Al	O
F-0	0.127	0.086	0.85	0.01	0.14	0.235
F-1	0.127	0.086	0.85	0.01	0.14	0.245
F-2	0.127	0.086	0.85	0.01	0.14	0.246
F-3	0.127	0.086	0.85	0.01	0.14	0.241
F-4	0.127	0.086	0.85	0.01	0.14	0.231
F-5	0.127	0.086	0.85	0.01	0.14	0.218
F-6	0.127	0.086	0.85	0.01	0.14	0.206

#### 4.3. Weld Pool Reaction

The Equilib module is applied to perform the modeling as follows [10]:

- In order to simulate the molten slag and steel phases, the FToxid, Fstel, and FactPS databases were utilized, with the solution phases of ASlag-liq all oxides, S (FToxid-SLAGH), and LIQUID (FStel-Liqu) being selected.
- The input metal chemistries were set based on the compositions provided in Table 4, while the flux compositions were based on those provided in Table 1.
- A modeling temperature of 2000 °C was established.
- The findings from the gas–slag–metal equilibrium model are detailed in our previous research [3].

#### 4.4. Assessment of Prediction Results

The predicted and measured manganese contents are plotted in Figure 4 against MnO addition level in flux. In Figure 4a, the manganese content predicted by the gas–slag–metal equilibrium model is indicated by the red star, while the manganese content predicted by the multi-zone model is indicated by the blue star. Figure 4b illustrates the predicted and the actual positions of the neutral point (NP). As was demonstrated in our previous studies, the manganese content tends to be significantly overestimated by the slag–metal equilibrium model due to overestimated MnO activity, in contrast to the gas–slag–metal equilibrium model [10,12]. However, even with the gas–slag–metal equilibrium model, the manganese content is still overestimated [12].

As can be seen in Figure 4a, the multi-zone model reduces the deviations between the predicted and the actual manganese contents compared to the gas–slag–metal equilibrium model, as indicated by the shaded red area in Figure 4a. A further explanation of the factors leading to the increased accuracy of the multi-zone model will be provided in Section 4.5.

Figure 4b illustrates the projected location of the NP, as determined by both the gas–slag–metal equilibrium model and the multi-zone model. The NP is defined as the point at which there is no further transfer of alloying elements between the flux and

WM [16,17].  $NP$  is an essential parameter in designing and specifying the MnO-bearing flux since it determines the alloying capacity of the manganese component [13,15]. If a flux formula is situated near the  $NP$  location, it is possible to regulate the manganese content in the WM by managing the manganese contents in both the BM and the electrode. The process for determining the  $NP$  location is consistent with the methodology that has been outlined in prior investigations [16,28]. As shown in Figure 4b, the  $NP$  predicted by the gas–slag–metal equilibrium model is at  $-1$  wt pct MnO, while the  $NP$  predicted by the multi-zone model is at 8 wt pct. The red and blue shaded regions demonstrate that, compared to the gas–slag–metal model, the multi-zone model decreases the disparity between the projected and the actual  $NP$  locations by 9 wt pct. Consequently, the multi-zone model, which accounts for the droplet, weld pool, and solidification zones, provides a superior prediction precision compared to the gas–slag–metal equilibrium model.

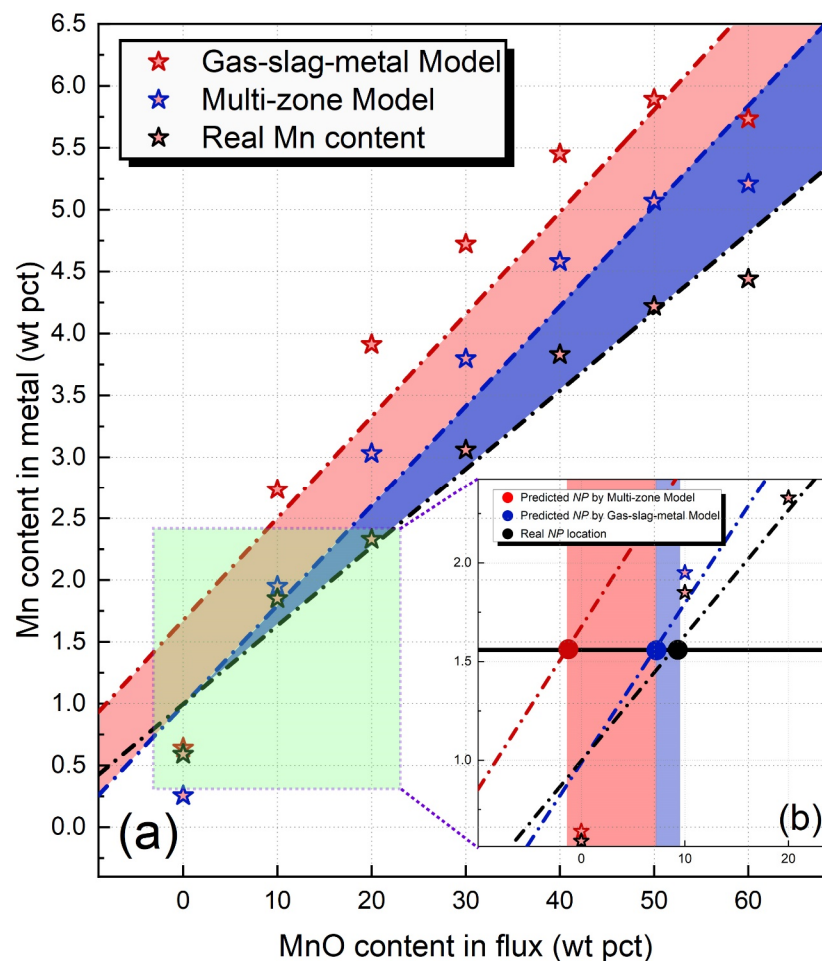


**Figure 4.** Predicted Mn content and NPs as a function of MnO content in flux: (a) predicted Mn content by equilibrium and multi-zone models, and (b) predicted location of NP by equilibrium and multi-zone models.

#### 4.5. Elemental Transfer Behavior and Model Parameters

In SAW engineering, the extent of loss or transfer of a specific element induced by flux is quantified by a  $\Delta$  quantity [4,5]. A positive  $\Delta$  value indicates an elemental gain from the flux, whereas a negative  $\Delta$  value indicates an elemental loss induced by the flux [15]. The manganese content in the weld metal (WM) can be expressed as Equation (8), as described in previous studies, where [pct Mn]<sub>N</sub> indicates the nominal composition of manganese and [pct Mn] indicates the composition of manganese in WM [10]:

$$[\text{pct Mn}] = [\text{pct Mn}]_N + \Delta\text{Mn} \quad (8)$$

Based on Equations (3) and (8), the value of  $\Delta\text{Mn}$  can be expressed as Equation (9), where  $[\text{pct Mn}]_N$  represents the nominal manganese content,  $\alpha_{\text{MnO}}$  represents the MnO activity, and  $[\text{pct O}]$  represents the predicted oxygen concentration in WM.

$$\Delta\text{Mn} = \frac{\alpha_{\text{MnO}}}{0.86 \cdot [\text{pct O}]} - [\text{pct Mn}]_N \quad (9)$$

Table 5 summarizes the MnO activity in both the gas–slag–metal equilibrium and the multi-zone models. The data in Table 5 indicate that the difference between the MnO activity in the gas–slag–metal equilibrium and multi-zone models is negligible. In order to further interpret the transfer behavior of manganese, the nominal manganese content and the predicted oxygen concentration are summarized and plotted in Figure 5.

**Table 5.** MnO activity in the gas–slag–metal equilibrium model and the multi-zone model.

Flux	Gas–Slag–Metal Equilibrium Model	Multi-Zone Model
F-1	$8.72 \times 10^{-2}$	$8.21 \times 10^{-2}$
F-2	$1.36 \times 10^{-1}$	$1.38 \times 10^{-1}$
F-3	$1.75 \times 10^{-1}$	$1.84 \times 10^{-1}$
F-4	$2.13 \times 10^{-1}$	$2.31 \times 10^{-1}$
F-5	$2.44 \times 10^{-1}$	$2.56 \times 10^{-1}$
F-6	$2.58 \times 10^{-1}$	$2.57 \times 10^{-1}$

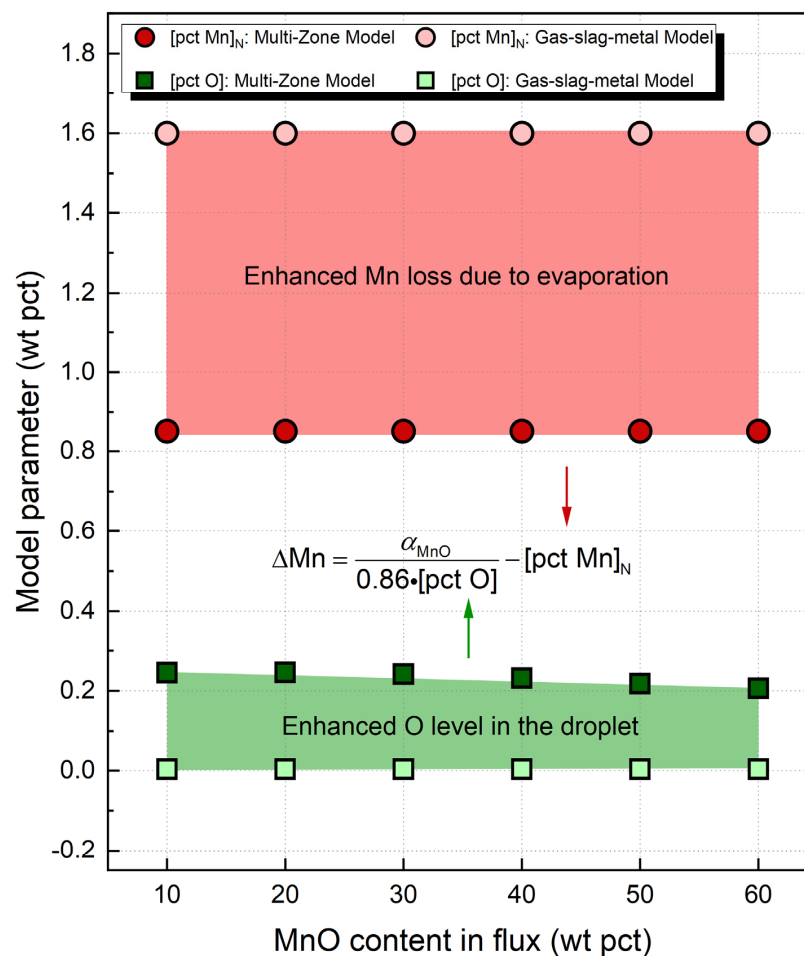


**Figure 5.** Model parameter pertinent to the level of  $\Delta\text{Mn}$ .

Figure 5 shows that the multi-zone model predicts a higher level of manganese loss due to evaporation and oxygen content in the droplet at the plasma–metal interface compared

to the gas–slag–metal equilibrium model, represented by the blue and red shaded regions, respectively. The evaporation of manganese from the weld pool during the SAW process has been extensively studied [14,25,28]. However, the gas–slag–metal equilibrium model overestimates the magnitude of  $[\text{pct Mn}]_N$  since it neglects the loss of manganese at the plasma–metal interface.

The gas–slag–metal equilibrium model underestimates the value of  $[\text{pct O}]$  because it does not consider the transfer of oxygen in the droplet zone [5]. To verify this hypothesis, the oxygen content change pathways in the metal, as projected by both the equilibrium and the multi-zone models, are illustrated in Figure 6. It is clear from Figure 6a,b that the trend of oxygen content variation in the metal is entirely dissimilar. In Figure 6a, the oxygen content stays constant during the tip and droplet phases, but then rises dramatically during the WM phase. Conversely, in Figure 6b, the oxygen content spikes during the droplet phase, but then decreases to a lower level during the WM phase.

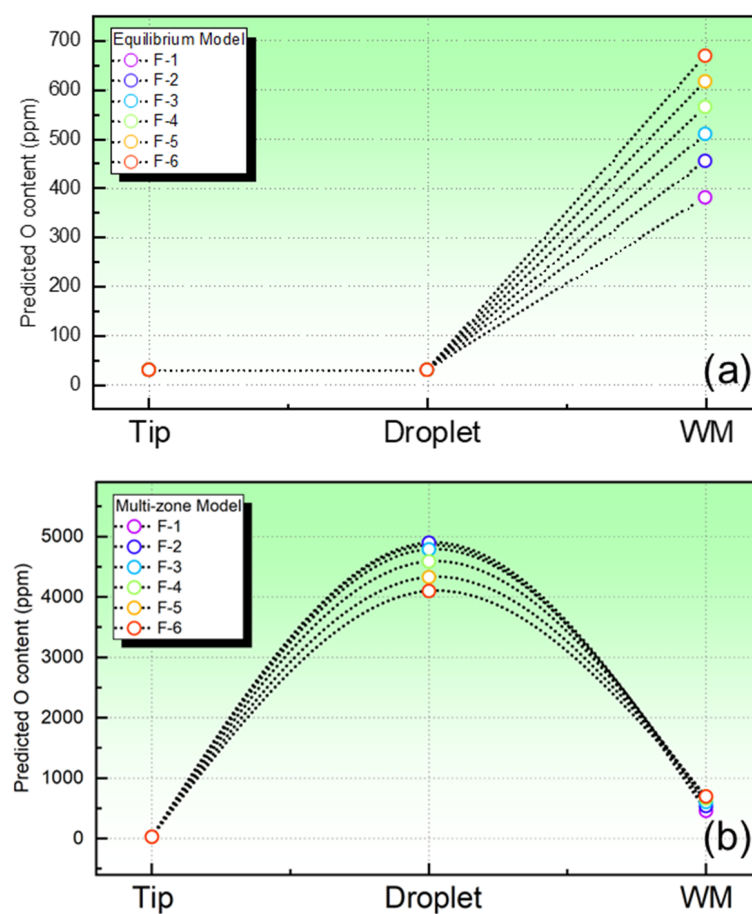


**Figure 6.** O content variation roadmaps in the metal predicted by both equilibrium and multi-zone models: (a) O content variation roadmap predicted by the equilibrium mode; (b) O content variation roadmap predicted by the multi-zone model.

Lau et al., and Polar et al. [34–36] sampled the droplet and revealed that the oxygen content in the droplet is in the order of 3000 ppm or more, which is much higher than that in the solidified WM. Therefore, the oxygen content in the droplet is significantly underestimated by the equilibrium model. The multi-zone model that has been proposed in this study, on the other hand, correctly forecasts the variation trend of oxygen in metal. Thus, from both experimental and theoretical perspectives, the consideration of oxygen transfer from the flux in the droplet zone is essential to improve the prediction accuracy for manganese.

#### 4.6. Analysis of Oxygen Potential

Due to the fact that the arc plasma and the weld pool are covered with a granular flux and molten slag, it is not feasible to gauge the gas compositions within the arc cavity [24]. Therefore, investigators have assumed that the oxygen level in the hot metal is proportional to the equilibrium partial pressure  $O_2$  in the arc cavity [13,34]. To verify this assumption, the predicted equilibrium partial pressure  $O_2$  is plotted against the measured oxygen content in the WM in Figure 7.

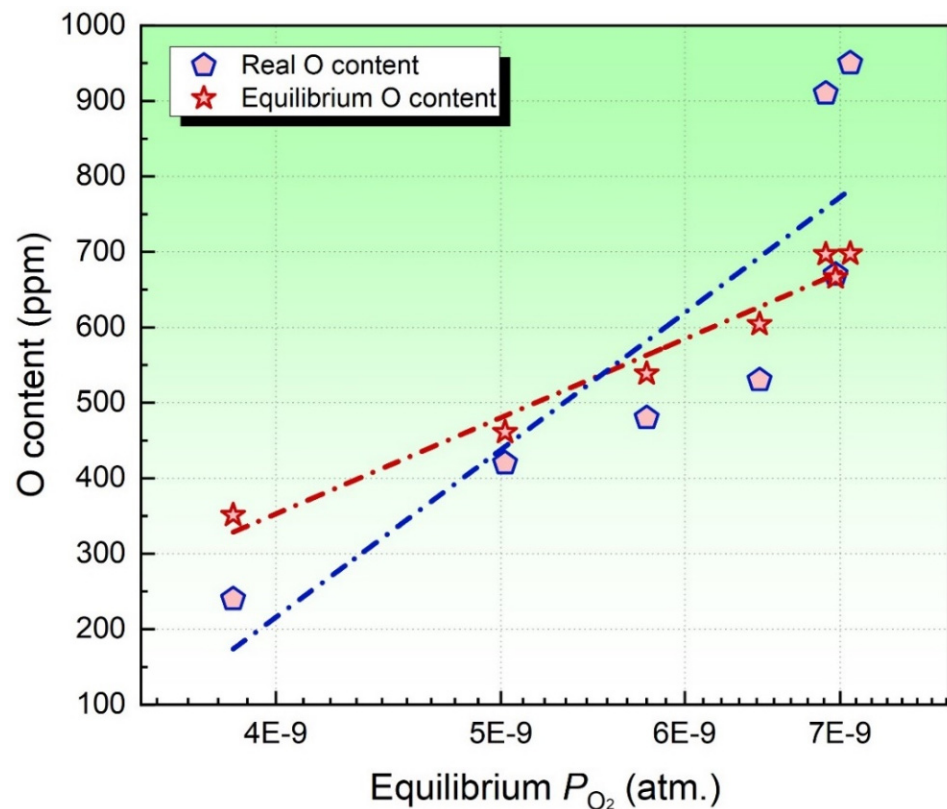


**Figure 7.** Relationship between equilibrium partial pressure of  $O_2$  and oxygen content.

As evidenced by Figure 7, an elevation in the equilibrium partial pressure of  $O_2$  generally yields an increase in the oxygen content. Consequently, taking into account the data from both past and present investigations, it can be postulated that the flux oxygen potential can be evaluated by considering the equilibrium partial pressure of  $O_2$  and the equilibrium oxygen content in the hot metal [10,24]. Notably, this assessment can be conducted without the requirement of experimental testing, thereby saving resources for flux design.

In summary, the gas–slag–metal equilibrium model overestimates  $\Delta Mn$  (the change in manganese content in the submerged arc welded metal enabled by MnO-bearing flux) due to overestimated [pct Mn]<sub>N</sub> and underestimated [pct O], resulting in a greater prediction error regarding the manganese content and the NP location. However, it should be noted that the manganese content is slightly overestimated, as shown by the green shaded area in Figure 4a. Previous studies have revealed that physical factors, especially oxide entrapment, may contribute to the oxygen content [34,35]. This improvement in oxygen level in the hot metal may enhance manganese loss by shifting Reaction (2) to the right side, thereby inducing deviations between the predicted and the actual manganese contents.

#### 4.7. The Application of the Model

It is well known that the MnO exert a significant impact on the microstructure and mechanical properties, as mentioned previously in this study. However, controlling the

composition through randomized experiments can be a significant waste of human and material resources. The model that has been proposed in this study may save experimental resources in terms of composition control, and enable welding technicians to predict welding compositions, particularly the regulation of MnO content on the weld metal composition. In addition,  $NP$  is an important parameter in flux design, and the model that has been proposed in this article presents a feasible method for accurately predicting the  $NP$  position, thus providing convenience for flux design.

This model may be extended to other welding modes, and we are also attempting to develop corresponding models. However, due to the differences in soldering methods, there are many important parameters that need to be adjusted, such as the existence state of the reaction interface, the temperature of the chemical reaction, and the definition of phases in the model. We will report on these models in future articles.

#### 4.8. The Limitations of the Model and Future Research Directions

This model is mainly established from a chemical perspective on the basis of oxygen layer theory, the Langmuir equation, and the equilibrium model. However, the physical interactions in arc welding can also have an impact on the composition, especially the increase in oxygen content in the droplet due to oxide entrapment from the flux. In addition, the kinetics of the welding process can affect the actual composition, particularly the degree of deviation from the thermodynamic equilibrium composition. Although it is assumed that arc welding reaches thermodynamic equilibrium locally, current technological limitations prevent us from determining the deviation between the real thermodynamic model and the assumed thermodynamic model. Therefore, in order to further improve the quality of the model, the following approaches may be necessary:

1. Introduce physical interactions and consider the effects of factors such as heat transfer, fluid mechanics, and oxide entrapment from the flux during the SAW process, to more accurately describe the phenomena in the welding process.
2. Introduce a suitable kinetic model to compensate for the bias between actual welding and the thermodynamic equilibrium state.

### 5. Conclusions

This study presents a multi-zone model to predict the manganese content in C-Mn steel welded with MnO-bearing flux in submerged arc welding. The accuracy of the model is verified using a comprehensive range of MnO-bearing fluxes, including acidic, neutral, and basic fluxes. Based on the study, the following conclusions can be drawn:

- i. Compared to the equilibrium model, the multi-zone model provides superior predictive accuracy for manganese content, flux oxygen potential, and  $NP$  location. Specifically, the multi-zone model reduces the deviation between the measured and the actual  $NPs$  from 11 to 2 wt pct.
- ii. The thermodynamic information and parameters in the model suggest that relying solely on the equilibrium in the weld pool zone results in overestimating the nominal manganese content while underestimating the oxygen content.
- iii. The multi-zone model is a more effective approach than the equilibrium model in accurately depicting the variations in oxygen content and manganese levels in the SAW process.

The main application range of this model is for the use of manganese–silicate fluxes in the SAW process. Manganese–silicate fluxes, with  $SiO_2$  and MnO as the main components, are particularly suitable for submerged arc welding of C-Mn steel. Common manganese–silicate fluxes include the following:  $CaF_2$ - $SiO_2$ -MnO flux,  $FeO$ - $SiO_2$ -MnO flux,  $CaO$ - $SiO_2$ -MnO flux,  $CaF_2$ - $SiO_2$ - $Al_2O_3$ -MnO flux, and  $CaO$ - $SiO_2$ - $Al_2O_3$ -MnO flux, etc. In practical applications, engineers usually select appropriate fluxes based on the electrode, BM, and welding requirements. Therefore, the model that has been proposed in this study may provide predictive information and theoretical guidance for matching welding materials, thereby saving production and manufacturing consumption.

**Author Contributions:** Conceptualization, J.Z. and D.Z.; methodology and software, J.Z. and D.Z.; funding acquisition, P.L. All authors have read and agreed to the published version of the manuscript.

**Funding:** This work was financially supported by National Natural Science Foundation of China (Grant No. 50474085), Initial Fund of Suqian University (Grant No. 2022XRC040), the Scientific Research and Innovation Team of Suqian University (Grant No. 2021td07), and Suqian Sci&Tech Program (Grant Nos. K202239 and K202122).

**Conflicts of Interest:** On behalf of all authors, the corresponding author states that there is no conflict of interest.

## References

1. Sengupta, V.; Havrylov, D.; Mendez, P. Physical Phenomena in the Weld Zone of Submerged Arc Welding—A Review. *Weld. J.* **2019**, *98*, 283–313. [[CrossRef](#)]
2. Bang, K.-s.; Park, C.; Jung, H.-c.; Lee, J.-b. Effects of flux composition on the element transfer and mechanical properties of weld metal in submerged arc welding. *Met. Mater. Int.* **2009**, *15*, 471–477. [[CrossRef](#)]
3. Zhang, D.; Shao, G.; Zhang, J.; Liu, Z. On the Moving of Neutral Point for Mn Subject to Submerged Arc Welding under Various Heat Inputs: Case Study into CaF<sub>2</sub>-SiO<sub>2</sub>-Na<sub>2</sub>O-MnO Agglomerated Fluxes. *Processes* **2022**, *10*, 1888. [[CrossRef](#)]
4. Olson, D.; Liu, S.; Frost, R.; Edwards, G.; Fleming, D. Nature and Behavior of Fluxes Used for Welding. *ASM Int. ASM Handb.* **1993**, *6*, 55–63. [[CrossRef](#)]
5. Natalie, C.A.; Olson, D.L.; Blander, M. Physical and Chemical Behavior of Welding Fluxes. *Annu. Rev. Mater. Sci.* **1986**, *16*, 389–413. [[CrossRef](#)]
6. AWS. *A 3.0 M/A3.0. Standard Welding Terms and Definitions*; AWS: Seattle, WA, USA, 2010.
7. Cho, D.-W.; Kiran, D.V.; Na, S.-J. Analysis of molten pool behavior by flux-wall guided metal transfer in low-current submerged arc welding process. *Int. J. Heat Mass. Transfer.* **2017**, *110*, 104–112. [[CrossRef](#)]
8. Cho, D.-W.; Song, W.-H.; Cho, M.-H.; Na, S.-J. Analysis of submerged arc welding process by three-dimensional computational fluid dynamics simulations. *J. Mater. Process. Technol.* **2013**, *213*, 2278–2291. [[CrossRef](#)]
9. Mitra, U.; Eagar, T. Slag-metal Reactions during Welding: Part I. Evaluation and Reassessment of Existing Theories. *Metall. Trans. B* **1991**, *22*, 65–71. [[CrossRef](#)]
10. Zhang, J.; Shao, G.; Fan, J.; Wang, L.; Zhang, D. A Review on Parallel Development of Flux Design and Thermodynamics Subject to Submerged Arc Welding. *Processes* **2022**, *10*, 2305. [[CrossRef](#)]
11. Zhang, J.; Peng, L.; Zhou, L.; Chen, Y. On the Si Content Prediction for Submerged Arc Welded Metal via Calphad Technique: A Brief Discussion. *J. Mater. Res. Technol.* **2022**, *21*, 1856–1862. [[CrossRef](#)]
12. Zhang, J.; Wang, L. Upgrading the prediction model for Mn content in submerged arc welded metal via CALPHAD technology: Case study into typical acidic and basic fluxes. *Ceram. Int.* **2022**, *49*, 6573–6579. [[CrossRef](#)]
13. Indacochea, J.E.; Blander, M.; Christensen, N.; Olson, D.L. Chemical Reactions During Submerged Arc Welding with FeO-MnO-SiO<sub>2</sub> Fluxes. *Metall. Trans. B* **1985**, *16*, 237–245. [[CrossRef](#)]
14. Chai, C.; Eagar, T. Slag Metal Reactions in Binary CaF<sub>2</sub>-Metal Oxide Welding Fluxes. *Weld. J.* **1982**, *61*, 229–232.
15. Burck, P.; Indacochea, J.; Olson, D. Effects of Welding Flux Additions on 4340 Steel Weld Metal Composition. *Weld. J.* **1990**, *3*, 115–122.
16. Chai, C.; Eagar, T. Slag-metal Equilibrium during Submerged Arc Welding. *Metall. Trans. B* **1981**, *12*, 539–547. [[CrossRef](#)]
17. Chai, C.-S. Slag-metal Reactions during Flux Shielded Arc Welding. Ph.D. Thesis, Massachusetts Institute of Technology, Cambridge, MA, USA, 1980.
18. Mills, A.; Thewlis, G.; Whiteman, J. Nature of inclusions in steel weld metals and their influence on formation of acicular ferrite. *Mater. Sci. Technol.* **1987**, *3*, 1051–1061. [[CrossRef](#)]
19. Minh, P.S.; Nguyen, V.-T.; Nguyen, V.T.; Uyen, T.M.T.; Do, T.T.; Nguyen, V.T.T. Study on the Fatigue Strength of Welding Line in Injection Molding Products under Different Tensile Conditions. *Micromachines* **2022**, *13*, 1890. [[CrossRef](#)]
20. Singh, M.; Sharma, S.; Muniappan, A.; Pimenov, D.Y.; Wojciechowski, S.; Jha, K.; Dwivedi, S.P.; Li, C.; Królczyk, J.B.; Walczak, D.; et al. In Situ Micro-Observation of Surface Roughness and Fracture Mechanism in Metal Microforming of Thin Copper Sheets with Newly Developed Compact Testing Apparatus. *Materials* **2022**, *15*, 1368. [[CrossRef](#)]
21. Liby, A.; Dixon, R.; Olson, D. *Welding: Theory and Practice*; Elsevier: Amsterdam, The Netherlands, 1990.
22. Chai, C.; Eagar, T. Prediction of weld-metal composition during flux-shielded welding. *J. Mater. Energy Syst.* **1983**, *5*, 160–164. [[CrossRef](#)]
23. Tuliani, S.; Boniszewski, T.; Eaton, N. Notch Toughness of Commercial Submerged Arc Weld Metal. *Weld. Met. Fabr.* **1969**, *37*, 327–339.
24. Zhang, J.; Shao, G.; Guo, Y.; Xu, Q.; Liu, Z. Facilitating Flux Design Process Geared Towards Submerged Arc Welding via Thermodynamic Approach: Case Study into CaF<sub>2</sub>-SiO<sub>2</sub>-Na<sub>2</sub>O-Al<sub>2</sub>O<sub>3</sub>-TiO<sub>2</sub> Agglomerated Flux. *Calphad* **2022**, *79*, 102483. [[CrossRef](#)]
25. Mitra, U. Kinetics of Slag Metal Reactions during Submerged Arc Welding of Steel. Ph.D. Thesis, Massachusetts Institute of Technology, Cambridge, MA, USA, 1984.

26. Mitra, U.; Eagar, T. Slag-metal Reactions During Welding: Part II. Theory. *Metall. Trans. B* **1991**, *22*, 73–81. [[CrossRef](#)]
27. Zhang, J.; Zhang, D. Thermodynamic Simulation of O Content Variation Roadmap in Submerged Arc Welding Process: From Droplet to Weld Metal. *Processes* **2023**, *11*, 784. [[CrossRef](#)]
28. Kou, S. *Welding Metallurgy*, 3rd ed.; JohnWiley & Sons, Inc.: Hoboken, NJ, USA, 2003; pp. 22–122.
29. Bale, C.W.; Bélisle, E.; Chartrand, P.; Decterov, S.; Eriksson, G.; Gheribi, A.; Hack, K.; Jung, I.-H.; Kang, Y.-B.; Melançon, J. Reprint of: FactSage Thermochemical Software and Databases, 2010–2016. *Calphad* **2016**, *55*, 1–19. [[CrossRef](#)]
30. Jung, I.-H. Overview of the Applications of Thermodynamic Databases to Steelmaking Processes. *Calphad* **2010**, *34*, 332–362. [[CrossRef](#)]
31. Block-Bolten, A.; Eagar, T.W. Metal vaporization from weld pools. *Metall. Trans. B* **1984**, *15*, 461–469. [[CrossRef](#)]
32. Zhu, J.; Wang, Y.; Shi, H.; Huang, L.; Mao, Z. Element loss behavior and compensation of additive manufacturing memory alloy. *Trans. China Weld. Inst.* **2022**, *43*, 50–55. [[CrossRef](#)]
33. Mitra, U.; Eagar, T. Slag Metal Reactions during Submerged Arc Welding of Alloy Steels. *Metall. Trans. A* **1984**, *15*, 217–227. [[CrossRef](#)]
34. Lau, T.; Weatherly, G.; McLean, A. Gas/metal/slag Reactions in Submerged Arc Welding Using CaO-Al<sub>2</sub>O<sub>3</sub> Based Fluxes. *Weld. J.* **1986**, *65*, 31–38.
35. Lau, T.; Weatherly, G.; McLean, A. The Sources of Oxygen and Nitrogen Contamination in Submerged Arc Welding using CaO-Al<sub>2</sub>O<sub>3</sub> Based Fluxes. *Weld. J.* **1985**, *64*, 343–347.
36. Polar, A.; Indacochea, J.; Blander, M. Electrochemically generated oxygen contamination in submerged arc welding. *Weld. J.* **1990**, *69*, 69–74.

**Disclaimer/Publisher’s Note:** The statements, opinions and data contained in all publications are solely those of the individual author(s) and contributor(s) and not of MDPI and/or the editor(s). MDPI and/or the editor(s) disclaim responsibility for any injury to people or property resulting from any ideas, methods, instructions or products referred to in the content.